

Loss-of-Function Mutations of Retromer Large Subunit Genes Suppress the Phenotype of an *Arabidopsis zig* Mutant That Lacks Qb-SNARE VTI11

Yasuko Hashiguchi,^a Mitsuru Niihama,^b Tetsuya Takahashi,^a Chieko Saito,^c Akihiko Nakano,^{c,d} Masao Tasaka,^a and Miyo Terao Morita^{a,1}

^a Graduate School of Biological Science, Nara Institute of Science and Technology, Ikoma, Nara 630-0101, Japan

^b Plant Genetics Laboratory, National Institute of Genetics, Mishima, Shizuoka 411-8540, Japan

^c Molecular Membrane Biology Laboratory, RIKEN, Wako 351-0198, Japan

^d Department of Biological Sciences, Graduate School of Science, University of Tokyo, Bunkyo-ku, Tokyo 113-0033, Japan

***Arabidopsis thaliana zigzag (zig)* is a loss-of-function mutant of Qb-SNARE VTI11, which is involved in membrane trafficking between the *trans*-Golgi network and the vacuole. *zig-1* exhibits abnormalities in shoot gravitropism and morphology. Here, we report that loss-of-function mutants of the retromer large subunit partially suppress the *zig-1* phenotype. Moreover, we demonstrate that three paralogous *VPS35* genes of *Arabidopsis* have partially overlapping but distinct genetic functions with respect to *zig-1* suppression. Tissue-specific complementation experiments using an endodermis-specific *SCR* promoter show that expression of *VPS35B* or *VPS35C* cannot complement the function of *VPS35A*. The data suggest the existence of functionally specialized paralogous *VPS35* genes that nevertheless share common functions.**

INTRODUCTION

Eukaryotic cells contain various endomembrane compartments that continuously communicate with each other and exchange materials through membrane trafficking. Membrane trafficking is essential for the transport of proteins and lipids to the appropriate sites of action in order to maintain the functions of organelles and to modulate higher-order cellular developmental processes. Analysis of the genomic sequence of *Arabidopsis thaliana* has revealed that several gene families involved in membrane trafficking are expanded in number relative to yeast or animal cells, including those that encode SNAREs (soluble NSF attachment protein receptors) and Rab GTPases, suggesting a more complex organization of endomembrane system than is found in other organisms (Rutherford and Moore, 2002; Sanderfoot, 2007).

Reverse genetics is a useful approach to study membrane trafficking in plant cells. However, the existence of paralogous genes often makes it difficult to study their physiological functions. Loss-of-function mutations of essential genes with or without redundancy tend to give rise to subtle phenotype or lethality, respectively. The functional significance of paralogous

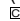
genes and the functional relationships between them are thus difficult to discern (Rojo and Denecke, 2008).

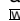
We have previously isolated the *Arabidopsis zigzag (zig)* mutant, a loss-of-function mutant of the gene encoding Qb-SNARE VPS10 interacting 11 (VTI11), and this mutant exhibits a defect in shoot gravitropism (Kato et al., 2002). The *zig-1* mutant exhibits additional morphological abnormalities: its inflorescence stem elongates in a zigzag fashion, and its leaves are small and wrinkled (Yamauchi et al., 1997). VTI11 is localized to the *trans*-Golgi network (TGN), the prevacuolar compartment (PVC), and vacuoles (Zheng et al., 1999; Uemura et al., 2004; Niihama et al., 2005). SNAREs are classified to subgroups (Qa-, Qb-, Qc-, and R-SNARE) according to amino acid sequences of the SNARE motif (Fasshauer et al., 1998). A correct complex composed of four SNAREs from each subgroup can lead to membrane fusion. VTI11 forms a complex with Qa-SNARE SYP22/SGR3/VAM3, Qc-SNARE SYP5, and R-SNARE VAMP727, probably at the PVC and vacuoles (Sanderfoot et al., 2001; Yano et al., 2003; Ebine et al., 2008). Because the molecular function of SNAREs is to aid in vesicle targeting and docking, their intracellular localization should be closely linked to their site of action (Cai et al., 2007). This indicates that VTI11 functions in membrane trafficking between the TGN and the PVC/vacuoles. Consistent with this idea, abnormal vacuolar structures have been observed in *zig-1* mutant cells (Morita et al., 2002).

Gravity is believed to be perceived by amyloplast sedimentation toward the direction of the gravitational force in the endodermal cell in *Arabidopsis* shoots (Fukaki et al., 1998; Morita and Tasaka, 2004). In *zig-1* shoots, amyloplasts in the endodermal cells do not sediment in the direction of gravity (Morita et al., 2002). Live cell imaging enabled us to show that functions and membrane dynamics of vacuoles closely correlate with

¹ Address correspondence to mimorita@bs.naist.jp.

The author responsible for distribution of materials integral to the findings presented in this article in accordance with the policy described in the Instructions for Authors (www.plantcell.org) is: Miyo Terao Morita (mimorita@bs.naist.jp).

 Some figures in this article are displayed in color online but in black and white in the print edition.

 Online version contains Web-only data.

www.plantcell.org/cgi/doi/10.1105/tpc.109.069294

amyloplast movement (Saito et al., 2005). We also found that *sgr3*, an amino acid substitution mutant of SYP22, exhibits reduced shoot gravitropism without any obvious morphological defects except for horizontal elongation of lateral shoots (Fukaki et al., 1996; Yano et al., 2003). Abnormalities are also found both in amyloplast sedimentation and in vacuolar structure in the endodermal cells of *sgr3* shoots. Furthermore, *sgr3*-type SYP22 exhibits a reduced ability to form a SNARE complex with VT111 and SYP5 (Yano et al., 2003). These results indicate that disruption of membrane trafficking to vacuoles in endodermal cells affects shoot gravitropism in *Arabidopsis*.

To elucidate the genetic network of membrane trafficking to vacuoles, we have performed a screen to identify mutants that can suppress the phenotype of *zig-1*. A dominant mutation *zig suppressor1* (*zip1*) could almost completely suppress the defects found in *zig-1* (Niihama et al., 2005). The mutation was localized to the *VT112* gene, which is a homolog of *VT111* (Niihama et al., 2005). Although *VT111* and *VT112* share 60% amino acid sequence identity and exhibit some functional redundancy, their intracellular localization and their SNARE partners differ (Sanderfoot et al., 1999; Zheng et al., 1999; Bassham et al., 2000; Surpin et al., 2003). We found that the *zip1* mutation likely imparts upon *VT112* the ability to substitute for the function of *VT111* by changing both the specificity of SNARE complex formation and its intracellular localization, suggesting a close functional relationship between these two *VT11* paralogs.

Here, we report a new *zig suppressor* mutant, *zip3*, which is a recessive mutant that partially suppresses both the gravitropism and morphological abnormalities of *zig-1*. A *zip3* single homozygous mutant itself does not exhibit a remarkable phenotype. *zip3* is a loss-of-function mutant of *VPS35A*, which is an ortholog of yeast *VPS35*, a component of the retromer involved in retrograde transport from the PVC/endosome to the TGN (Seaman et al., 1997). Recent studies in plants have demonstrated that the *Arabidopsis* genome contains three *VPS35* paralogs referred to as A, B, and C (Shimada et al., 2006; Jaillais et al., 2007) that share redundant functions in plant viability (Yamazaki et al., 2008). We report here a distinct functional divergence between these three *VPS35* paralogs with respect to their ability to suppress the *zig-1* phenotype.

RESULTS

Phenotypic Characterization of the *zip3* Mutant of *zig-1*

The *zig-1* mutant exhibits abnormal morphology, including a zigzag-shaped inflorescence stem, small wrinkled leaves, and abnormal shoot gravitropism (Yamauchi et al., 1997; Kato et al., 2002). *zip3-1* was isolated as a suppressor mutant of *zig-1* from ethyl methanesulfonate-mutagenized *zig-1* seeds (Niihama et al., 2005). The angles between adjacent internodes in the second metamer of *zip3-1 zig-1* were smaller than those of *zig-1* but larger than those of wild-type plants (Figures 1A to 1C; see Supplemental Figure 1A online). Consistently, the length of the internodes in the second metamer (internodes between the adjacent lateral branches and between the youngest leaf and the first lateral branch of the main shoot) and parameters of leaf

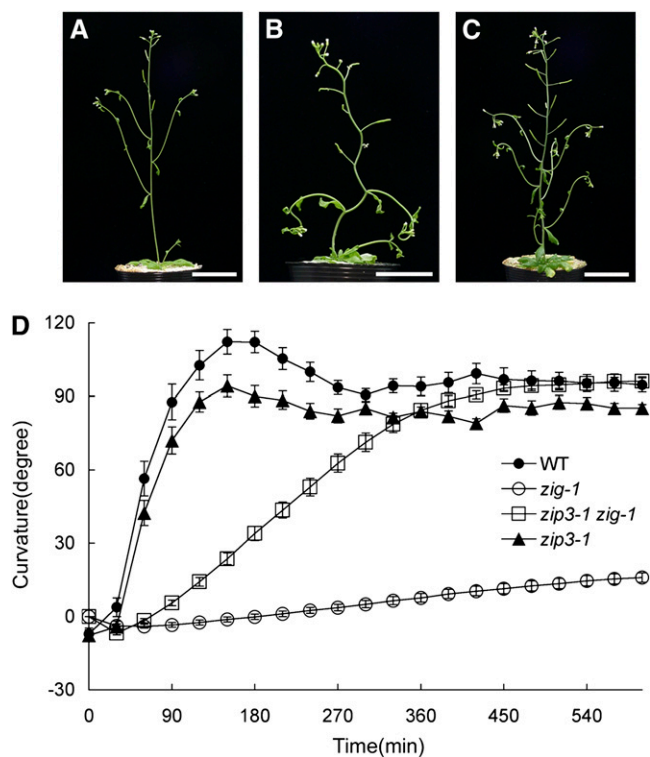


Figure 1. Phenotypes of the *zip3-1 zig-1* Double Mutant.

(A) to (C) Six-week-old plants of wild type (A), *zig-1* (B), and *zip3-1 zig-1* (C). Bars = 3 cm.

(D) Gravitropic phenotypes of the wild type (closed circles), *zig-1* (open circles), *zip3-1* (closed triangles), and *zip3-1 zig-1* (open squares). After 5-week-old plants were placed horizontally at 23°C under dim nondirectional light, inflorescence curvature was measured at 30-min intervals. Twenty individuals of each genotype were examined. Bars represent SE. [See online article for color version of this figure.]

shape in the *zip3-1 zig-1* suppressor mutants were of intermediate value compared with those of the wild type and the *zig-1* mutant (see Supplemental Figures 1B and 1C online). In a study of shoot gravitropism, when wild-type inflorescence stems were placed horizontally (gravistimulation), they bent upwards and became nearly perpendicular within ~90 min (Figure 1D). As reported previously, *zig-1* inflorescence stems showed little response (Figure 1D; Yamauchi et al., 1997). By contrast, stems of the *zip3-1 zig-1* double mutant showed reduced but significant shoot gravitropism, with the curvature of the inflorescence stems reaching a perpendicular position within 6 h after gravistimulation (Figure 1D). The *zip3-1* single mutant showed nearly normal shoot gravitropism. These results demonstrate that *zip3-1* partially suppresses both the morphological and gravitropic phenotypes of *zig-1*.

ZIP3 Encodes *VPS35A*

F2 progeny derived from a cross between *zip3-1 zig-1* (Columbia [Col] background) and *zig-3* (Wassilewskija background) were used to map *ZIP3* to the middle of chromosome 2. We next

mapped *ZIP3* more finely using F2 progeny derived from a cross between *zip3-1 zig-1* and a hybrid line *zig-Ler* (Landsberg *erecta*; see Methods). By analyzing 446 independent F2 progeny of the latter cross, the location of the *ZIP3* locus was narrowed to a region between a polymorphic marker on BAC F5J6 and that on BAC T13L6. We found a single G-to-A substitution in one open reading frame (*At2g17790*), resulting in nonsense mutation at the twelfth Trp (W12; Figure 2A). By sequencing *At2g17790* from an additional *zip zig-1* mutant with a similar phenotype derived from the same screen for *zig-1* suppressor mutants, we identified an allele, *zip3-2*, bearing a nonsense mutation at R200 (see Supplemental Figures 2A, 2C, and 2F online). Furthermore, two T-DNA insertion lines (SALK_125271 and SALK_039689) were crossed to *zig-1*, allowing us to confirm that both T-DNA insertion mutations are able to suppress the *zig-1* phenotype (see Supplemental Figures 2A and 2D to 2F online).

A 7.2-kb wild-type genomic fragment containing the *At2g17790* open reading frame, predicted promoter region (1.4 kb), and 3' downstream region (0.3 kb) was cloned and introduced into *zip3-1 zig-1* plants for a complementation test (Figure 2A). Inflorescence stems of eight independent T2 lines of the resulting transgenic plants exhibited abnormal stem morphology and very reduced gravitropism with similar kinetics as the parental *zig-1* single mutant (Figures 2B and 2C). Taken together, these results demonstrate that *ZIP3* is *At2g17790*. *At2g17790* was previously reported to encode *VPS35A* (Jaillais et al., 2007). In The Arabidopsis Information Resource, *ZIP3* (*At2g17790*) is annotated as a protein similar to vacuolar protein sorting-associated protein 35 (*Vps35*) family proteins.

In *Saccharomyces cerevisiae*, *Vps35p* is a component of the large subunit of the retromer that is required for protein recycling from the PVC/endosomes to the TGN. *Vps26p* and *Vps29p* constitute the large subunit together with *Vps35p*. Components of the retromer large subunit are highly conserved in eukaryotes (Bonifacino and Rojas, 2006). *Arabidopsis* has three *VPS35* genes (*ZIP3/VPS35A*, *At2g17790*; *VPS35B*, *At1g75850*; and *VPS35C*, *At3g51310*), two *VPS26* genes (*VPS26A*, *At5g53530*; *VPS26B*, *At4g27690*; Jaillais et al., 2007), and one *MAIGO1/VPS29* gene (*At3g47810*; Shimada et al., 2006).

Since *zip3-1* is a nonsense mutation at Trp-12, it is most likely to be a null mutant allele. We confirmed by immunoblot analysis using anti-*VPS35A* (kindly provided by I. Hara-Nishimura) that *VPS35A* protein is not detected in *zip3-1* or any of the other alleles (see Supplemental Figure 3 online). Considering the similar phenotype of the *zip3 zig-1* alleles (see Supplemental Figure 2 online), they all appear to represent loss-of-function mutants of *VPS35A*. In addition, each single mutant allele showed no obvious phenotype for either gravitropism or stem morphology (see Supplemental Figure 4 online).

***zip3-1* Also Suppresses the Cytological Phenotype of *zig-1* in Endodermal Cells**

Plastids accumulating dense starch granules, called amyloplasts, are thought to act as statoliths in gravity sensing by higher plants (Sack, 1991). In wild-type *Arabidopsis* shoots, endodermal cells appear to serve as the gravity-sensing cells and contain amyloplasts that sediment in the direction of gravity (Figure 3A; Fukaki

et al., 1998). By contrast, amyloplasts do not sediment in the endodermal cells of *zig-1*, *sgr3*, and *sgr3/grv2/kam2* mutants (Figure 3B; Morita et al., 2002; Yano et al., 2003; Silady et al., 2004), suggesting that vacuolar functions mediated by TGN-PVC/vacuole membrane trafficking are important for amyloplast sedimentation. Interestingly, the majority of amyloplasts sedimented toward the direction of gravity in the *zip3-1 zig-1* mutant (Figure 3C). To evaluate amyloplast sedimentation more quantitatively, the number of amyloplasts positioned at the upper, middle, or bottom region of endodermal cells was counted using embedded longitudinal sections, as shown in Figures 3A to 3D (see Supplemental Table 1 online). Although most amyloplasts were observed at the bottom region in the wild type and *zip3-1* single mutants, amyloplasts were observed in all regions in *zig-1* cells. By contrast, a majority of the amyloplasts was observed at the bottom region, with a smaller but significant number at the upper region in *zip3-1 zig-1* cells (see Supplemental Table 1 online). Therefore, partial suppression of the gravitropic phenotype of *zig-1* by *zip3-1* mutation appears to correlate with the extent of amyloplasts sedimentation in endodermal cells.

Using electron microscopy, we previously observed that wild-type endodermal cell amyloplasts are enclosed by a vacuolar membrane with a thin cytoplasmic layer, whereas *zig-1* amyloplasts are not enclosed by such a membrane and appear to be more localized toward the cell periphery (Figures 3E and 3F). By contrast, the amyloplasts in *zip3 zig-1* cells are surrounded by a vacuolar membrane, although clusters of abnormal vesicles were occasionally observed (Figure 3G). To evaluate the extent of suppression of the *zig-1* phenotype by *zip3*, we quantitatively analyzed cytological manifestations of the suppressed phenotype, including amyloplast movement and vacuolar membrane dynamics using live endodermal cells (Figures 3H to 3K). For these studies, we used the autofluorescence of the plastid and green fluorescent protein (GFP) fluorescence (following the expression of a GFP- γ -TIP fusion localized to vacuolar membrane) to visualize amyloplasts and the vacuolar membrane, respectively. We compared various physical characteristics of the amyloplasts and vacuolar membrane in wild-type and mutant endodermal cells (see Supplemental Table 2 online).

In all aspects, such as the number of amyloplasts enclosed by a vacuolar membrane, amyloplast and vacuolar dynamics, and the presence of an abnormal vesicular structure, *zip3-1 zig-1* cells exhibited values that were intermediate between those of wild-type and *zig-1* cells (see Supplemental Table 2 online). Thus, the *zip3-1* suppressor mutation appears to partially restore the functional integrity of the vacuoles, suggesting that the *zip3* mutation may partially restore a defect in membrane trafficking caused by loss-of-function of *ZIG/VTI11*. Moreover, the intermediate recovery of the cytological *zig-1* phenotype by the *zip3-1* mutation correlates with partial suppression of the gravitropic phenotype (Figure 1). When *ZIP3/VPS35A* was specifically expressed in the endodermis of *zip3-1 zig-1* using the *SCARECROW* (*SCR*) promoter (Wysocka-Diller et al., 2000), the resulting transgenic plants (eight independent T2 lines) showed reduced gravitropism similar in level to the *zig-1* single mutant (Figures 2D and 2E). This indicates that vacuolar integrity in the endodermal cells supported by membrane trafficking is closely linked to gravitropism of the inflorescence stems.

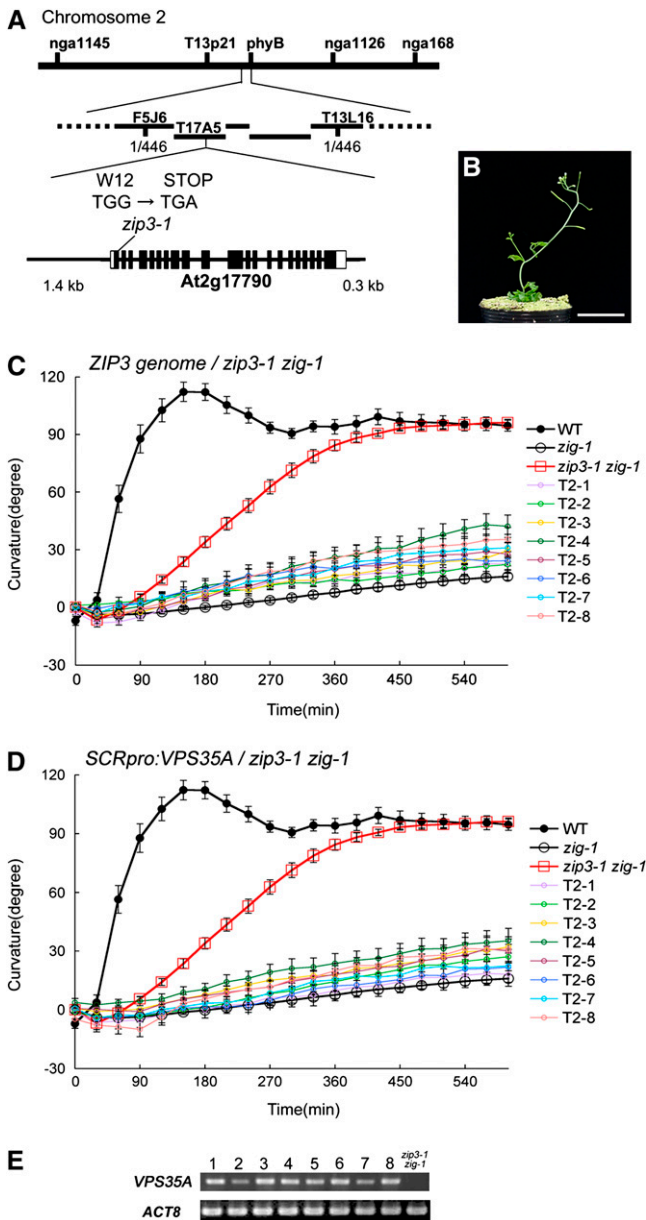


Figure 2. ZIP3 Is VPS35A.

(A) The ZIP3 locus was mapped between two cleaved-amplified polymorphic sequence markers, F5J6 and T13L16 on chromosome 2. A nonsense mutation was found at the twelfth Trp in the *At2g17790* gene in the *zip3-1 zig-1* mutant. The gene structure of *At2g17790* is shown schematically; exons are indicated by boxes (open boxes, untranslated region; closed boxes, coding regions), and introns are indicated by lines between boxes.

(B) and (C) Complementation analysis.

(B) Aerial part of 5-week-old *zip3-1 zig-1* T2 plant bearing the *At2g17790* genomic fragment indicated in (A). Note that it shows a *zip3-1*-like phenotype. Bar = 3 cm.

(C) Gravitropic response of wild-type (closed circles), *zip3-1 zig-1* (red open squares), *zig-1* (open circles), and eight independent T2 lines of *zip3-1 zig-1* containing the *At2g17790* genomic fragment (T2-1 to T2-8; open colored circles). Ten individuals of each transgenic line were

How Does the *zip3* Mutation Suppress *zig-1*?

To address this question, we focused on *VTI12*, a paralog of *ZIG/VTI11*, since we have found that *VTI12* is involved in suppression in the case of *zip1 zig-1* (Niihama et al., 2005). *VTI11* interacts with SYP22 on the PVC/vacuole, whereas *VTI12* forms a complex with SYP4 on the TGN in wild-type cells (Sato et al., 1997; Zheng et al., 1999; Sanderfoot et al., 1999, 2001; Uemura et al., 2004). *zip1*, a gain-of-function mutation of *VTI12*, altered the intracellular localization and SNARE partner of *VTI12*, resulting in the substitution of *zip1*-type *VTI12* for *VTI11*. In addition, over-expression of wild-type *VTI12* can suppress the *zig-1* phenotype, depending on its expression level (Surpin et al., 2003), probably due to the ability of wild-type *VTI12* to substitute for *VTI11*.

These results prompted us to test whether *VTI12* is also involved in suppression of the *zig-1* phenotype in *zip3-1 zig-1* cells. We analyzed whether *VTI12* interacts with SYP22 using anti-SYP22 antibody to immunoprecipitate protein from extracts prepared from the inflorescence stem from *zig-1*, *zip3 zig-1*, and *zip1 zig-1* plants (Figure 4). In *zig-1* plants, little *VTI12* protein formed SNARE complexes with SYP22, indicating that wild-type *VTI12* has some ability to interact with SYP22, but it was not sufficient to substitute for *VTI11* function (Niihama et al., 2005). In addition, we confirmed that 2.5-fold more SYP22 was coimmunoprecipitated with *VTI12* in *zip1 zig-1* extracts compared with *zig-1*, as a positive experimental control (Niihama et al., 2005). In *zip3-1 zig-1* extracts, a slightly increased amount of *VTI12* was coimmunoprecipitated with SYP22, although the increase was not statistically significant (Figure 4).

Dysfunction of the Retromer Large Subunit Suppresses the *zig-1* Phenotype

The molecular lesion found in *zip3-1* demonstrates that a loss-of-function mutation of *ZIP3/VPS35A*, which probably causes dysfunction of the retromer containing *VPS35A*, suppressed the *zig-1* phenotype. To test whether mutations in other large subunits can be suppressors of *zig-1*, we crossed *zig-1* to *mag1-1*, a T-DNA insertion allele of *VPS29*, in which the expression level of *VPS29* is much lower than in the wild type (Shimada et al., 2006). The *mag1-1* single mutant showed reduced but significant gravitropism probably due to its thin stem and reduced growth rate (Figure 5A). *mag1-1 zig-1* showed a significant gravitropic response comparable to that of the parental *mag1-1* single mutant (Figure 5A). We note that *mag1-1* suppressed the gravitropic phenotype of *zig-1* to a greater extent than did *zip3-1*. The fact that

examined. Bars represent SE.

(D) and (E) Endodermis-specific expression of *VPS35A* extinguished the suppressive effect of *zip3-1* on the *zig-1* phenotype.

(D) Gravitropic response of wild-type (closed circles), *zip3-1 zig-1* (red open squares), *zig-1* (open circles), and independent eight T2 lines of *zip3-1 zig-1* containing *SCRpro:ZIP3/cVPS35A* (T2-1 to T2-8; open colored circles). Ten individuals of each transgenic line were examined. Bars represent SE.

(E) Expression of *ZIP3/VPS35A* derived from the transgene was confirmed by RT-PCR analyses of the eight transgenic lines. Analysis of the untransformed double mutant line is shown in the lane at the far right.

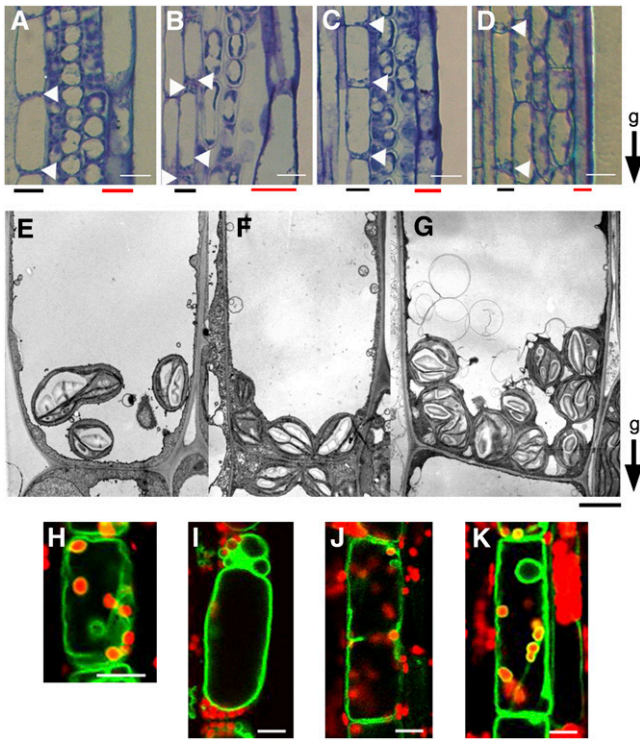


Figure 3. Endodermis of Inflorescence Stems.

(A) to (D) Longitudinal sections of inflorescence stems (~2 to 3 cm below the apex) of the wild type (A), *zig-1* (B), *zip3-1 zig-1* (C), and *zip3-1* (D). The growth orientation of stems was maintained during fixation. g, direction of gravity; red bars, epidermis; black bars, endodermis. Arrowheads indicate location of amyloplasts in endodermal cells. Bars = 20 μ m.

(E) to (G) Electron microscopy of endodermal cell of the wild type (E), *zig-1* (F), and *zip3-1 zig-1* (G). g, direction of gravity. Bars = 2 μ m.

(H) to (K) Confocal images of amyloplasts and vacuolar membrane in living endodermal cells. The wild type (H), *zig-1* (I), *zip3-1 zig-1* (J), and *zip3-1* (K). Amyloplasts and vacuolar membranes were observed using chlorophyll autofluorescence from plastids (red) and GFP fluorescence from GFP- γ -TIP (green), respectively. The transgenic line expressing GFP- γ -TIP under the control of the SCR promoter (Saito et al., 2005) was crossed with each mutant. The result of quantitative analysis based on this observation is shown in Supplemental Table 2 online.

the morphological phenotype of *mag1-1 zig-1* was similar to that of the *mag1-1* single mutant indicates that *mag1-1* can suppress the morphological phenotype of *zig-1* (see Supplemental Figure 5 online). Thus, the loss-of-function mutation in *VPS29*, a retromer component other than *VPS35*, can also suppress the *zig-1* phenotype and the fact that its suppressive effect is greater than that of *zip3* is likely due to the former being a single copy gene.

In the *Arabidopsis* genome, there are two paralogs of the gene encoding the other large subunit of retromer, *VPS26*. Since *mag1-1* can suppress *zig*, mutations in either *VPS26A*, *VPS26B*, or both are expected to suppress the *zig-1* phenotype. We next crossed T-DNA insertion lines (*vps26a*, GABI_053C12; *vps26b*, SALK_142592) with *zig-1* (Figure 5B). We could not detect full-length transcripts from either gene by RT-PCR analysis of total

RNA from the corresponding insertion mutant (Figure 5C), indicating that these are loss-of-function mutants. Both single mutants were indistinguishable from the wild type both in stem morphology and in gravitropism (see Supplemental Figure 6 online). As expected, *vps26a* suppressed the *zig-1* phenotype (Figures 5D and 5F). The gravitropic response of *vps26a zig-1* inflorescence stems was greater than that of *zip3-1 zig-1* stems but lesser than that of *vps26a* single mutant stems, suggesting that suppression by *vps26a* is partial. Interestingly, *vps26b* did not suppress the *zig-1* phenotype at all (Figures 5E and 5F), suggesting that the genetic functions of *vps26a* and *vps26b* differ with respect to suppression of *zig-1*. These results demonstrate that loss-of-function mutations of components of the retromer large subunit, *ZIP3/VPS35A*, *VPS29* and *VPS26A*, suppress the *zig-1* phenotype. This suggests a close relationship between these three proteins, implying that *VPS35A*, *VPS29*, and *VPS26A* constitute a retromer large subunit. Furthermore, our results indicate

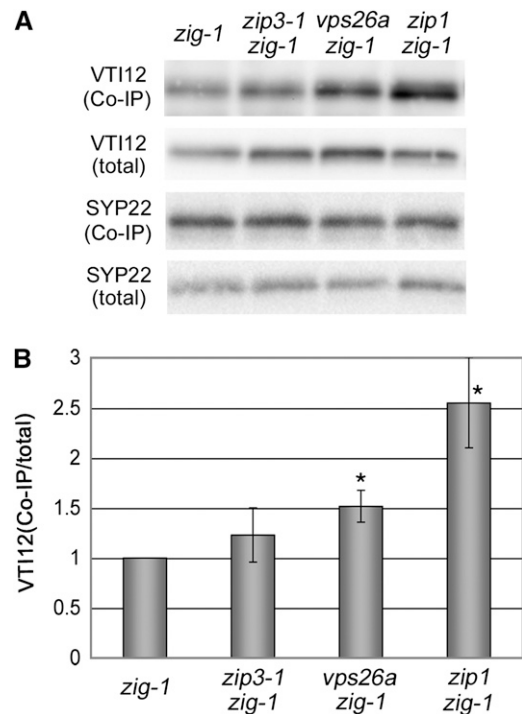


Figure 4. Interaction between SYP22 and VT112.

(A) Immunoprecipitation analysis using anti-SYP22 antiserum with *zig-1*, *zip3-1 zig-1*, *vps26a zig-1*, and *zip1 zig-1* plant extracts. Proteins were extracted from inflorescence stems of 6-week-old plants. VT112 and SYP22 in immunoprecipitates were detected by immunoblotting using anti-VT112 antiserum and anti-SYP22 antiserum, respectively (first and third panels from top). The total amounts of VT112 and SYP22 are also indicated (second and fourth panels from top).

(B) The relative incorporation ratio of VT112 into the SNARE complex containing SYP22 (immunoprecipitated VT112/ total VT112) was calculated based on results shown in (A). Average values of four independent experiments are presented with error bars showing SD. Values were normalized to that of *zig-1* plants. Quantification of the band intensity was performed with the software Sion Image. The statistical significance against *zig-1* control was tested using a Student *t* test (**P* < 0.05).

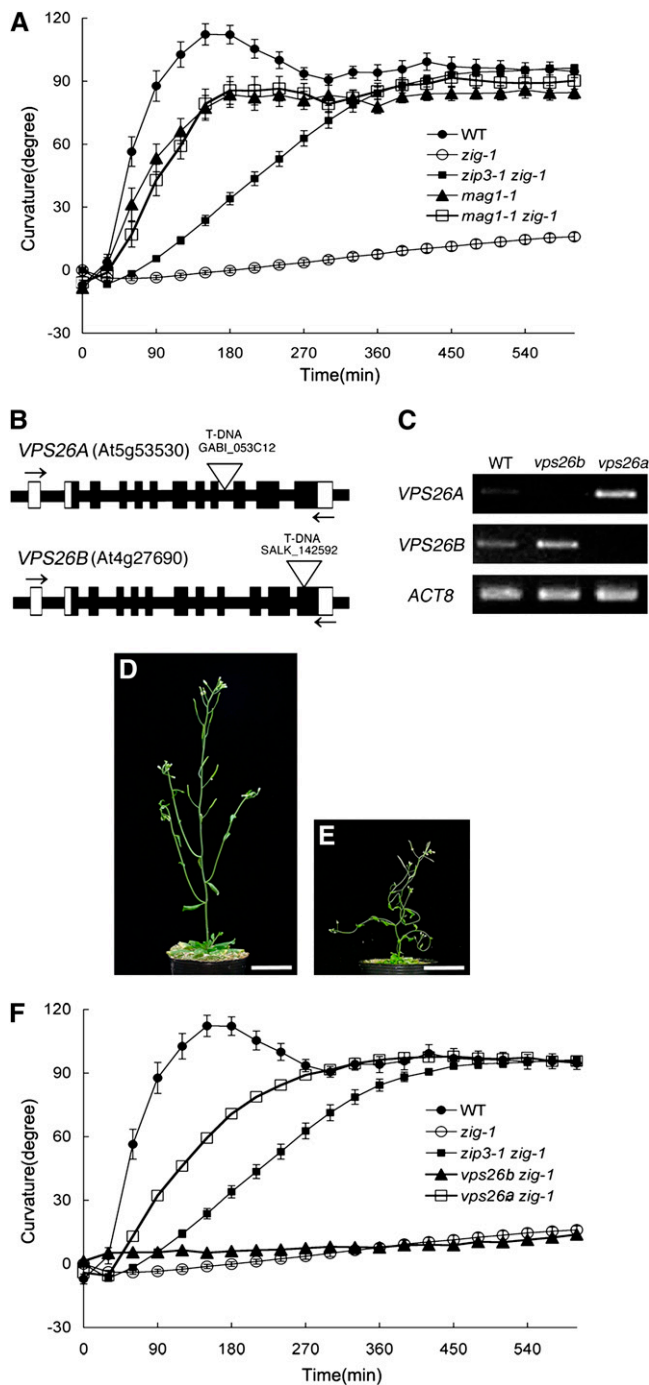


Figure 5. Suppressive Effect of Loss-of-Function Mutations in Components of the Retromer Large Subunit.

(A) Gravitropic response of the wild type (closed circles), *zip3-1 zig-1* (closed squares), *zig-1* (open circles), *mag1-1* (closed triangles), and *mag1-1 zig-1* (open squares). At least 15 individuals of each genotype were examined. Bars represent SE.

(B) Schematic structures of *VPS26A* and *VPS26B* genes and positions of T-DNA insertions. Boxes indicate exons, and white regions represent untranslated regions. Open triangles show positions of T-DNA insertions. Arrows indicate the position of primers used for RT-PCR analyses in **(C)**.

that dysfunction of the retromer can suppress the *zig-1* phenotype caused by loss-of-function mutation of Qb-SNARE VTI11.

Since the suppressive effect of *vps26a* was greater than that of *zip3-1*, we tested whether *vps26a* can affect VTI12-SYP22 complex formation. We performed immunoprecipitation analyses on extracts prepared from *vps26a zig-1* plants (Figure 4). Interestingly, significantly increased amount of VTI12 coimmunoprecipitated with SYP22 from *vps26a zig-1* extracts compared with that from *zig-1* extracts. This result strongly suggests that VTI12-SYP22 complex formation is promoted by the *vps26a* mutation. We note that the amount of VTI12 coimmunoprecipitated with SYP22 correlates with the extent of suppression by each mutation, though the increase found in *zip3-1 zig-1* was not statistically significant (*zip3-1* < *vps26a* < *zip1*; Figures 1 and 5; Niihama et al., 2005). This result suggests that dysfunction of the retromer large subunits suppresses the *zig-1* phenotype by promoting VTI12-SYP22 complex formation.

Functional Relationship among Paralogs of *VPS35*

The two *VPS26* paralogs in the *Arabidopsis* genome may share redundant function for plant viability, since we were unable to generate a *vps26a vps26b* double mutant, at least for the allele combination we tested (data not shown). Interestingly, however, the roles of *vps26a* and *vps26b* with respect to suppression of the *zig-1* phenotype appear to differ, as shown in Figures 5D to 5F. Thus, we postulate that our suppressor screen allowed us to discern subtle functional differences between redundant paralogous genes and the physiological significance of these differences.

There are three *VPS35* paralogs in *Arabidopsis*. We next investigated the functional relationship between the *VPS35* paralogs by genetic analysis. T-DNA insertion lines (*vps35b*, SALK_014345; *vps35c*, SALK_099735) were crossed with *zig-1* (Figure 6A). We were unable to detect full-length transcripts from each gene by RT-PCR performed on RNA isolated from the corresponding mutant (Figure 6B), indicating that these are loss-of-function mutants. As was the case for *vps26*, both *vps35b* and *vps35c* single mutants themselves showed no obvious phenotype in either stem morphology or gravitropism (see Supplemental Figure 7 online). Interestingly, neither *vps35b* nor *vps35c* was able to suppress the *zig-1* phenotype (Figures 6C to 6E). This result indicates that the genetic functions of *VPS35B* and *VPS35C* differ from that of *VPS35A* with regard to the suppression of the *zig-1* phenotype.

To further investigate redundancy between the three paralogs, we analyzed the ability of double mutations in *VPS35* paralogs to suppress the gravitropic phenotype of *zig-1*. Inflorescence stems from *vps35b vps35c zig-1* plants exhibited poor gravitropism,

(C) RT-PCR analysis to detect expression of *VPS26A* or *VPS26B* in wild-type and mutant plants using the primers indicated by arrows in **(B)** **(D)** and **(E)** Morphological phenotypes of 6-week-old plants of *vps26a zig-1* **(D)** and *vps26b zig-1* **(E)**. Bars = 3 cm.

(F) Gravitropic response of wild-type (closed circles), *zip3-1 zig-1* (closed squares), *zig-1* (open circles), *vps26a zig-1* (open squares), and *vps26b zig-1* (closed triangles). At least 15 individuals of each genotype were examined. Bars represent SE.

[See online article for color version of this figure.]

similar to that observed for the *zig-1* single mutant (Figure 6F), consistent with what was observed for *vps35b zig-1* or *vps35c zig-1* double mutants (Figure 6E). By contrast, combination of either *vps35b* or *vps35c* mutation with the *zip3-1 zig-1* genotype (*zip3-1 vps35b zig-1* or *zip3-1 vps35c zig-1*) increased the gravitropic response. However, the response of *zip3-1 vps35b zig-1* exhibited a biphasic curve with the first phase of the response (within 3 h) appearing faster than that of *zip3-1 zig-1*. Both *vps35b* and *vps35c* appear to enhance the suppressive effect of *zip3-1*, although the suppressive effect of *vps35b* is much weaker than that of *vps35c*. These results suggest that there is some genetic redundancy between the *VPS35* paralogs with respect to suppression of the *zig-1* phenotype.

Protein Functions of the VPS35 Paralogs Are Unlikely to Be Equivalent

The genetic function of the *VPS35* paralogs appeared to be distinct but somewhat overlapping. Although each paralog is ubiquitously expressed in all organs examined (Schmid et al., 2005), we do not know whether their level of expression is similar in all tissues or cells. Thus, we cannot determine whether the subtle differences in genetic function might be explained by differential patterns of expression of the paralogs or whether they might reflect differences in their molecular function. To address this question, *VPS35B* or *VPS35C* was expressed under the control of the endodermis-specific *SCR* promoter (*SCRpro:VPS35B* or *SCRpro:VPS35C*) in the *zip3-1 zig-1* genetic background (Figure 7).

As shown in Figure 2D, when *ZIP3/VPS35A* was expressed from the *SCR* promoter in *zip3-1 zig-1* plants, the resulting transgenic plants exhibited a poor gravitropic response that was similar to the response observed in the *zig-1* single mutant. If *VPS35B* and *VPS35C* have similar molecular functions as *ZIP3/VPS35A*, then the gravitropic response of the resulting transgenic plants would be predicted to be similar to that observed in *zig-1* plants. However, *SCRpro:VPS35B* showed no effect on the gravitropic response of *zip3-1 zig-1* plants, even though the transgene was clearly expressed in the plants, suggesting that molecular function of *VPS35B* differs at least partially from that of *ZIP3/VPS35A* (Figures 7A and 7B).

With respect to *SCRpro:VPS35C*, the transgenic lines exhibited a gravitropic response that was similar to that observed in *zip3-1 zig-1* or *SCRpro:VPS35B/zip3-1 zig-1* plants, although slight differences in the response were observed in independent lines (Figure 7C and 7D). Therefore, neither *VPS35B* nor *VPS35C* can substitute for *ZIP3/VPS35A* at least when expressed from the same promoter. These results suggest that the protein functions of *VPS35B* or *VPS35C* are distinct from those of *ZIP3/VPS35A* in the endodermis.

DISCUSSION

Functional Deficiency of the Retromer Large Subunit Suppresses the Loss-of-Function Mutant of Qb-SNARE VTI11, *zig-1*

Here, we demonstrate that *zip3*, which partially suppresses the morphological and gravitropic phenotype of *zig-1*, is a loss-

of-function mutation of *VPS35A* (Figures 1 and 2; see Supplemental Figure 1 online). It is an ortholog of the yeast *Vps35* gene, which is a component of the retromer large subunit functioning in the retrieval of the CPY (carboxypeptidase Y) sorting receptor (*Vps10*) to the Golgi from the PVC/endosome (Seaman et al., 1997). The retromer is composed of two subcomplexes: *Vps26p-Vps29p-Vps35p*, a heterotrimeric large subunit involved in cargo recognition, and the *Vps5p-Vps17p* complex promoting vesicle formation (Seaman et al., 1998; Nothwehr et al., 2000). All components, except for *Vps17p*, are highly conserved in higher eukaryotes. The human ortholog of *Vps5p*, termed sorting nexin 1 (*SNX1*) (Kurten et al., 1996; Horazdovsky et al., 1997; Nothwehr and Hindes, 1997), and other *SNX* family members are thought to function in a role similar to the *Vps5p-Vps17p* subcomplex (Bonifacino and Hurley, 2008).

In the *Arabidopsis* genome, retromer orthologs have been reported (Jaillais et al., 2006, 2007; Oliviusson et al., 2006; Shimada et al., 2006; Yamazaki et al., 2008). The presence of components of the large subunit (*VPS26A*, *VPS29*, and *VPS35C*) on the multivesicular body (MVB) has been demonstrated by immunoelectron microscopy (Oliviusson et al., 2006). Each loss-of-function yeast mutant lacking a retromer component exhibits a similar phenotype, such as mis-sorting of the CPY out of the cell (Horazdovsky et al., 1997; Nothwehr and Hindes, 1997; Seaman et al., 1997; Nothwehr et al., 1999; Reddy and Seaman, 2001). Similarly, all three *Arabidopsis* mutants, T-DNA insertion mutants of *VPS26A* or *VPS35A* and *mag1-1* with reduced expression of *VPS29*, partially suppressed the *zig-1* phenotype (Figure 5). The result suggests that *VPS26A*, *VPS29*, and *VPS35A* share the same molecular function, as part of the large subunit of the retromer in wild-type plants. Consistent with our genetic analysis, a recent study using the yeast two-hybrid analysis has shown that *VPS35A* can physically interact with *VPS29* and *VPS26A* in yeast (Jaillais et al., 2007).

Possible Mechanism of *zig-1* Suppression by Loss of Function of the Retromer

We previously reported that *VTI12*, a paralog of *VTI11*, can suppress the *zig-1* phenotype. Genetic analysis has demonstrated that *VTI11* and *VTI12* have redundant functions, at least in part. Our previous data suggested that an excess amount of wild-type *VTI12* or *zip1*-type *VTI12* forms a SNARE complex with *SYP22* leading to a functional substitution of the *VTI11-SYP22* complex (Surpin et al., 2003; Niihama et al., 2005). We assumed that the mechanism of suppression in the case of loss-of-function mutants of the retromer could be explained by a similar scenario. However, amount of the *VTI12-SYP22* SNARE complex was slightly increased but not significant in *zip3-1 zig-1* compared with that detected in *zig-1* plants used as a control (Figure 4).

By contrast, we detected a significant increase of *VTI12-SYP22* complex formation in *vps26a zig-1* (Figure 4). Unfortunately, we could not perform this experiment in *mag1-1 zig-1* plants due to poor growth. *VTI12-SYP22* complex formation was much more robust in *zip1 zig-1* plants used as a positive control as reported previously (Niihama et al., 2005). The extent of suppression of the gravitropic phenotype of these *zip zig-1*

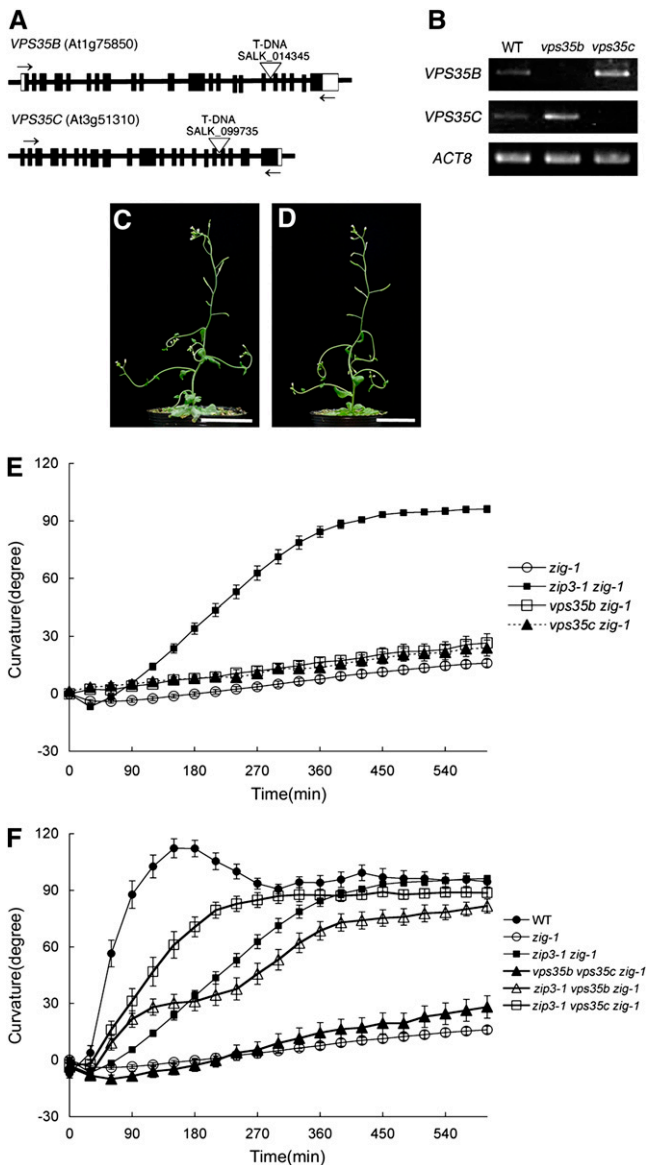


Figure 6. Suppressive Effect of Loss-of-Function Mutations in *VPS35* Paralogs.

(A) Schematic structures of *VPS35B* and *VPS35C* genes and positions of T-DNA insertions. Boxes indicate exons, and white regions represent untranslated regions. Open triangles show positions of T-DNA insertions. Arrows indicate the position of primers used for RT-PCR analyses to detect expression of *VPS35B* or *VPS35C* in **(B)**.

(B) RT-PCR analysis to detect expression of *VPS35B* or *VPS35C* in wild-type and mutant plants using the primers indicated by arrows in **(A)**.

(C) and **(D)** Morphological phenotypes of 6-week-old plants of *vps35b zig-1* **(C)** and *vps35c zig-1* **(D)**. Bars = 3 cm.

(E) Gravitropic response of *zip3-1 zig-1* (closed squares), *zip-1* (open circles), *vps35b zig-1* (open squares), and *vps35c zig-1* (closed triangles). At least 15 individuals of each genotype were examined. Bars represent SE.

(F) Gravitropic response of wild-type (closed circles), *zip3-1 zig-1* (closed squares), *zip-1* (open circles), *zip3-1 vps35b zig-1* (open triangles), *zip3-1 vps35c zig-1* (open squares), and *vps35b vps35c zig-1* (closed triangles). At least 15 individuals of each genotype were examined. Bars represent SE.

mutants positively correlated with the amount of the VT112-SYP22 complex: *zip1 zig-1* > *vps26a zig-1* > *zip3 zig-1*. Our results suggest that VT112-SYP22 complex formation is one of the mechanisms underlying suppression of the *zig-1* phenotype through loss of function of the retromer, as is the case of *zip1 zig-1*. If so, how could dysfunction of the retromer promote VT112-SYP22 complex formation? In wild-type cells, VT112 is mainly localized to the TGN, and a fraction of VT112 is localized to SYP22-positive PVC. Such dual localization of VT112 suggests cycling of VT112 between the TGN and the PVC (Uemura et al., 2004).

Retrieval trafficking from the PVC to the TGN is performed by the retromer. The retromer components VPS29, VPS26, and VPS35 are localized to the PVC/MVB (Oliviusson et al., 2006; Jaillais et al., 2007; Yamazaki et al., 2008). Phenotypes observed in retromer mutants, such as mis-sorting of vacuolar seed storage proteins to the extracellular space and increased accumulation of VSR receptors, indicate that the plant retromer is indeed involved in cargo retrieval from the PVC to the TGN in *Arabidopsis* (Shimada et al., 2006; Yamazaki et al., 2009). If we suppose that VT112 reaching the PVC is immediately retrieved by the retromer, then we might expect that dysfunction of the retromer might lead to mis-sorting of VT112 to the PVC and/or vacuole. This provides a possible explanation: in *zip3 zig-1*, *vps26a zig-1*, or *mag1-1 zig-1* plants, VT112 mis-sorted to the PVC and/or vacuoles due to dysfunction of the retromer could form a SNARE complex with SYP22 in the absence of VT111, resulting in partial substitution of VT111-SYP22 function.

We tested whether VT112 is mislocalized to the PVC in *zip3-1 zig-1* by analyzing colocalization between GFP-VT112 and ARA6-RFP in endodermal cells (see Supplemental Figure 8 online). However, significant mislocalization of GFP-VT112 to the ARA6-RFP-positive PVC could not be detected in *zip3-1 zig-1* and *zip3-1* compared with the wild type and *zip-1*. This could be due to the only partial suppressive ability of *zip3-1*. Alternatively, the result suggests that VT112-SYP22 complex formation is promoted by a secondary effect of dysfunction of the retromer (e.g., disorganization of endomembrane system in the retromer mutants could result in increase of VT112-SYP22 complex formation).

Possibly, the increase of the VT112-SYP22 complex may not be the primary cause of the suppression. The loss-of-function of retromer may cause a detrimental effect not only on retrieval of specific cargos but also on retrieval of membrane lipids to the TGN, and this may result in accumulation of mis-sorted membrane to central vacuoles. Mis-sorting of membrane to vacuoles could recover vacuolar dynamics required for dynamic movement of amyloplasts in endodermal cells in *zip3-1 zig-1* (Figure 3).

Functional Differences among Paralogs of *VPS35*

Arabidopsis has one *VPS29*, two *VPS26*, and three *VPS35* genes. It has been reported that the *vps29* null allele shows severe, pleiotropic effects on plant development and growth (Jaillais et al., 2007; Shimada et al., 2006). *VPS35* function is

At least 15 individuals of each genotype were examined. Bars represent SE.

[See online article for color version of this figure.]

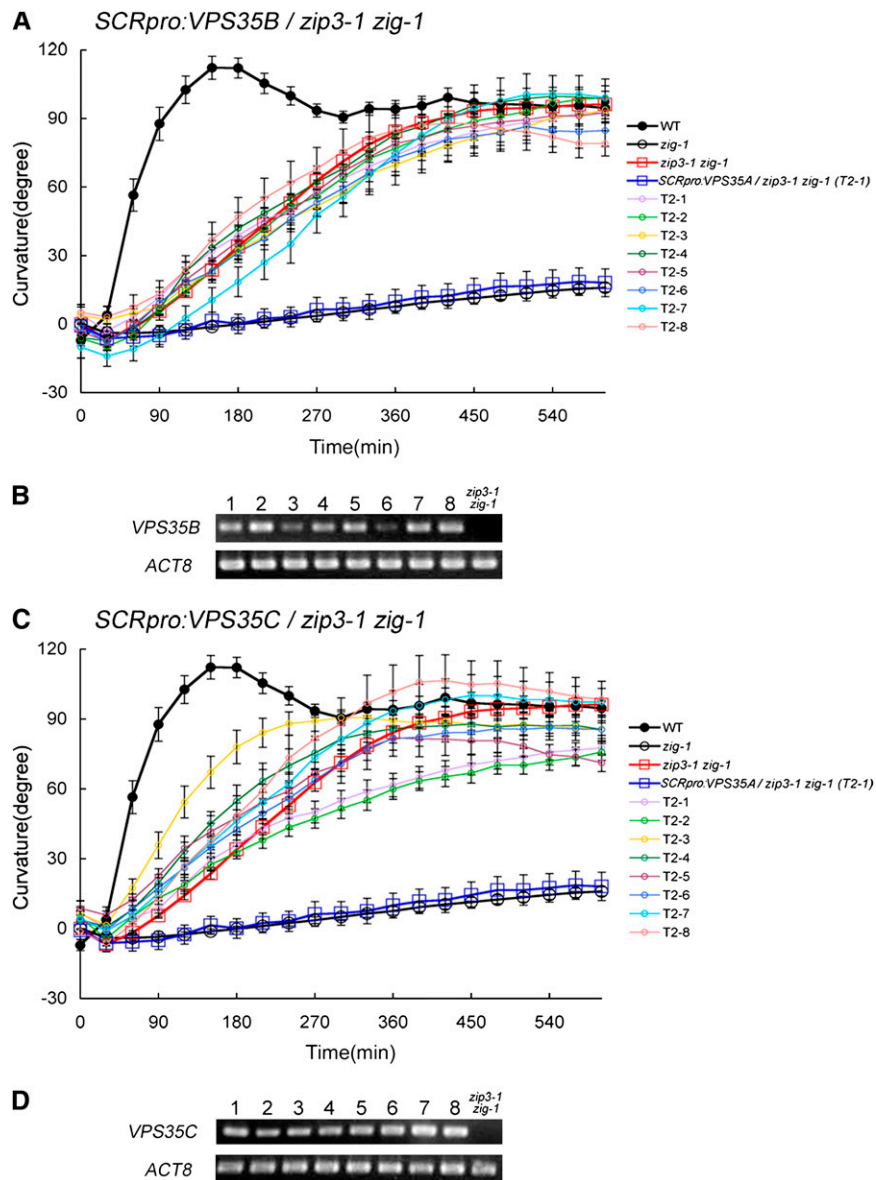


Figure 7. Endodermis-Specific Expression of VPS35B or VPS35C in *zip3-1 zig-1* Cells.

(A) and **(C)** Gravitropic response of wild-type (closed circles), *zip3-1 zig-1* (red open squares), *zip3-1* (open circles), *SCRpro:VPS35A/zip3 zig-1* (blue open squares), and eight independent T2 lines of *zip3-1 zig-1* plants containing *SCRpro:VPS35B* **(A)** or *SCRpro:VPS35C* **(C)** (T2-1 to T2-8; open colored circles). Ten individuals of each transgenic line were examined. Bars represent SE.

(B) and **(D)** Expression of *VPS35B* **(B)** or *VPS35C* **(D)** derived from the transgene was confirmed by RT-PCR analyses of the eight transgenic lines in each case.

probably essential because it has not been possible to generate a triple null mutant, *vps35a vps35b vps35c* (Yamazaki et al., 2008). We were unable to generate a *vps26a vps26b* double mutant from the F2 population (data not shown). By contrast, none of the *vps35a*, *-b*, or *-c* or *vps26a* or *vps26b* single mutants shows any obvious phenotype (see Supplemental Figures 6 and 7 online; Yamazaki et al., 2008). These results indicate that the paralogous genes of *VPS35* and *VPS26* have redundant functions regarding plant viability.

However, our genetic analysis revealed that *VPS26A* and *VPS26B* have distinct genetic functions with respect to suppression of the gravitropic phenotype of *zip3-1*, since *vps26a* but not *vps26b* could suppress *zip3-1* (Figures 5D to 5F). Similarly, *VPS35A* also showed a distinct genetic function from its paralogs with regard to *zip3-1* suppression (Figures 6C to 6E). Analysis of the triple mutants (*vps35b vps35c zip3-1*, *zip3-1 vps35b zip3-1*, and *zip3-1 vps35c zip3-1*) revealed a subtle functional relationship between the paralogs. The fact that *vps35b* and *vps35c*

enhanced the suppressive effect of *zip3* subtly and greatly, respectively, indicates that the genetic function of *ZIP3/VPS35A* and *VPS35C* are distinct but overlapping with respect to *zig-1* suppression (Figure 6E).

Our genetic analysis implies partially overlapping but distinct functions of *VPS35* paralogs. Such differences in genetic function, however, could result from differences in the expression pattern of each paralog. Meanwhile, all *VPS35* genes are ubiquitously expressed in various organs (Schmid et al., 2005), although we have not analyzed the expression pattern of each gene at the tissue level. A tissue-specific complementation test using the *SCR* promoter demonstrated that expression of neither *VPS35B* nor *VPS35C* in the endodermis negates the suppressive effect of *zip3* on the gravitropic phenotype (Figure 7). By contrast, expression of *VPS35A* by the same promoter did complement the effect of *zip3*, as expected (Figures 2D and 2E). We cannot exclude the possibility that all *VPS35* proteins might share the same molecular function, but only *VPS35A* is stable in the endodermis of *zip3-1 zig-1* background. However, these results indicate that *VPS35B* or *VPS35C* cannot substitute for the functions of *ZIP3/VPS35A* in mediating gravitropism in the endodermis, at least when expressed at similar levels of transcripts by the same promoter. Taken together, our results suggest that not only the genetic function but also the protein function of *VPS35B* or *VPS35C* is partially different from that of *VPS35A*.

How do the functions of the gene products of the *VPS35* paralogs differ from each other? One possibility is a difference in recognition of cargo for retrograde trafficking, since *VPS35* is the subunit responsible for binding to the cytoplasmic domains of cargo proteins (reviewed in Seaman, 2005; Collins, 2008). Analysis of the crystal structure of the C-terminal domain of human *VPS35* (Hiero et al., 2007) in addition to secondary structure prediction strongly suggests that the entire *VPS35* protein adopts an α -helical solenoid structure containing 17 HEAT-like helical repeats (Collins, 2008). It has been suggested that multiple regions of *VPS35* are involved in binding to a cargo protein (Seaman, 2007; Canuel et al., 2008). In addition, the fact that distinct domains within yeast *VPS35p* mediate the retrieval of two different cargo proteins (Nothwehr et al., 1999) implies that the retromer may be able to associate with multiple cargo proteins at the same time (Collins, 2008).

In *Arabidopsis*, *VPS35A* shares 67 and 70% identity in amino acid sequence with *VPS35B* and *VPS35C*, respectively. Such a difference may give rise to variety in selectivity of cargo proteins. Another possibility is that the gene product of each *VPS35* paralog may act as a retromer within distinct membrane compartments or subdomains. Although *VPS35* has been shown to be localized to the PVC/MVB in plant cells (Oliviusson et al., 2006; Yamazaki et al., 2008), localization of each *VPS35* paralog remains to be elucidated. It has been suggested that *VPS26p* recruits *VPS35p* to the membrane in yeast (Reddy and Seaman, 2001). Recent studies using mammalian cells suggest that formation of the entire heterotrimeric core is a prerequisite for membrane attachment (Collins et al., 2008). Attachment of the retromer core to the membrane is dependent upon the action of the membrane-associated SNX proteins (Rojas et al., 2007). Human *VPS35* also binds to the SNX proteins, and other retromer components, in addition to *VPS26* and *VPS29* (Haft et al., 2000).

These studies indicate that association with other retromer components including SNX proteins is important for recruitment of *VPS35* to sites of action, implying that binding of each *VPS35* paralog to other proteins or a combination of the components may affect the site of action of *VPS35* in *Arabidopsis*. The above two possibilities do not seem to be mutually exclusive. *VPS35A* could differ from *VPS35B* with regard to cargo selectivity and/or intracellular localization. It might share some such functions with *VPS35C*, given the partial overlap of genetic function between *VPS35A* and *VPS35C*.

Recent phylogenetic studies suggest that several components of systems of membrane trafficking evolved through gene duplication and specialization (Dacks and Field, 2007; Dacks et al., 2008). Divergence of gene families encoding key factors of membrane trafficking, such as SNAREs and Rab GTPases, suggests a complexity of the endomembrane organization in plant cells. The functions of divergent gene family members have been suggested to be redundant, based on a subtle mutant phenotype or on the lethality of multiple mutants. Paralogous genes probably share ancestral functions but may have since developed distinct individual functions. Determining the precise individual functions of each paralog is a challenge because such functions are subtle, cryptic, and difficult to discern beyond being explained by simple genetic redundancy. The distinct and/or partially overlapping functions of the *VPS35* paralogs reported here provide an example of the elucidation of such complexity. To elucidate more precisely the molecular mechanisms underlying functional differences between *VPS35* paralogs, further investigations will be required. Variation in combinations of retromer complexes including SNX proteins, their intracellular localization, and cargo selectivity should be clarified in planta in the future. In addition, functional interaction between the retromer and its regulatory factors, such as Rab5 and Rab7, which has recently been suggested in animal cells (Rojas et al., 2008), during plant development is an important issue.

Shoot Gravitropism Is a Sensitive Indicator of the Status of Post-Golgi Trafficking in Endodermal Cells

The endodermis is the major site of gravity perception in the *Arabidopsis* shoot, and amyloplasts are thought to be statoliths that sediment toward the direction of gravity within the endodermal cell (Fukaki et al., 1998; Saito et al., 2005). In *zig-1* cells, amyloplasts do not sediment but are positioned at the cell periphery even within the upper portion of the cell (Morita et al., 2002). In addition, vacuole formation and function in the mutant are affected, and a dynamic vacuolar structure, including transvacuolar strands and the membrane surrounding the amyloplasts, are not observed in *zig-1* cells (Saito et al., 2005). A similar vacuolar and amyloplast phenotype is observed in other *sgr* mutants, such as *sgr2*, *sgr3*, and *sgr8/grv2*. All of the genes responsible for these mutants have been suggested to be involved in post-Golgi membrane trafficking (Kato et al., 2002; Morita et al., 2002; Yano et al., 2003; Silady et al., 2004; Shimoi et al., 2005; Tamura et al., 2007; Kanamori et al., 2008; Silady et al., 2008).

ZIP3 also encodes a protein that is probably involved in retrograde transport from the PVC to the TGN. As we showed

here, amyloplast sedimentation was almost normal (Figure 3), and vacuolar and amyloplasts dynamics in the endodermal cells were partially recovered in *zip3 zig-1* plants (Figure 3). This partial suppression of the cytological phenotype in the endodermal cells correlates with the partial suppression of the physiological phenotype on gravitropism (Figure 1). Consistently, *zip1* completely suppresses the *zig-1* gravitropic phenotype as well as the cytological phenotype (Niihama et al., 2005). We have already demonstrated that the gravitropic defect in *zig-1* plants can be attributed to the lack of VTI11 function in the endodermis (Morita et al., 2002). Expression of *VPS35A* under the control of the *SCR* promoter complemented the gravitropic suppression phenotype in *zip3 zig-1* plants (Figures 2D and 2E), indicating that effect of the *zip3* mutation on the endodermal cells is the cause of the suppression of the gravitropic phenotype. Taken together, we conclude that the gravitropic phenotype strongly correlates with aberrant post-Golgi membrane trafficking in endodermal cells.

Using this feature of endodermal cells, we found that the retromer, composed of *VPS26A-VPS29-VPS35A*, is genetically involved in the function of VTI1 family members. Moreover, this approach uncovered functional differences between paralogous genes, which are cryptic in the absence of the *zig-1* mutation. Although the endodermis is nonessential for *Arabidopsis* viability, it is essential for gravity sensing. Therefore, we can use the gravitropic phenotype as a sensitive marker to monitor the status of membrane trafficking in endodermal cells. Our genetic strategy is useful to unravel the molecular network of membrane trafficking in plant cells that is thought to have complex endomembrane organization.

METHODS

Plant Materials and Growth Conditions

The Col-0 accession of *Arabidopsis thaliana* was used as the wild type. *zig-1 sgr4-1* is also a Col-0 accession, and both *zip3-1 zig-1* and *zip3-2 zig-1* were isolated from an M2 population of *zig-1* seeds mutagenized with ethyl methanesulfonate (Niihama et al., 2005). *zip3-3* (SALK_039689), *zip3-4* (SALK_125271), *vps26a* (GABI_053C12), *vps26b* (SALK_142592), *vps35b* (SALK_014345), and *vps35c* (SALK_099735) were from the SALK T-DNA insertion collection (Col-0). mRNA expression of each gene in the corresponding mutant was examined by RT-PCR analysis using specific primer sets (cVPS35B-F2/-R2, cVPS35C-F2/-R2, cVPS26A-F1/-R2, and cVPS26B-F1/-R2; see Supplemental Table 3 online for their sequence). *mag1-1* was kindly provided by I. Hara-Nishimura (Shimada et al., 2006). Seeds were surface sterilized with 5% sodium hypochlorite solution and then plated on Murashige and Skoog plates (1 × MS salt mixture, 1% [w/v] sucrose, 0.01% [w/v] myoinositol, 0.05% [w/v] gellan gum, and 0.05% MES-KOH, pH 5.7) followed by treatment at 4°C for 2 d. Seedlings were transplanted and grown on soil (mixture of vermiculite from Nittai and Metromix G550 from Sun Gro Horticulture covered with Ube Perlite Type I from Ube Kosan) under constant white light at 23°C.

Gravitropism Assay

To examine the gravitropic responses of inflorescence stems, intact 5-week-old plants with primary stems 4 to 8 cm in length were placed horizontally under nondirectional dim light at 23°C. Photographs were taken at indicated times, and then stem curvature was measured on the digital image with Image J (<http://rsb.info.nih.gov/ij/>) as the angle

formed between the growing direction of the apex and the horizontal base line.

Mapping *zip3*

Based on the previous study, we had noticed *Ler* accessions contain natural variations that suppress the *zig-1* phenotype to some extent. Since they behaved as quantitative trait loci, a mapping population generated by a cross between *Ler* and *zip3-1 zig-1* should cause confusion. Thus, we first isolated F2 progeny from a cross between *Ler* and *zig-1*, which contained a homozygous *zig-1* mutation and exhibited an obvious *zig-1* phenotype. This renders suppressive factors in the *Ler* background negligible. Each inbred line was examined with polymorphic markers to select specific lines that contained a pair of or a region of chromosomes homozygously derived from *Ler* (*zig-1Ler* lines). Meanwhile, we roughly determined the *ZIP3* locus on chromosome II using an F2 mapping population generated by cross between *zig-3* derived from Wassilewskija accession and *zip3-1 zig-1* because there is no suppressive factor in the Wassilewskija background. To map *ZIP3* finely, we prepared a mapping population from a cross between *zip3-1 zig-1* and a specific *zig-1 Ler* line containing a homozygous *Ler* region largely derived from the *Ler* ecotype on chromosome II. For fine-scale mapping, DNA was prepared from ~220 F2 progeny. We made cleaved-amplified polymorphic sequence markers that can recognize polymorphisms between Col and *Ler* based on information provided by The Arabidopsis Information Resource.

Histological Analysis

For observation of endodermal cells, stem segments were fixed, embedded in Technovit7100, and sectioned as described previously (Morita et al., 2002). For electron microscopy, the samples of inflorescence stem were embedded in Spurr's resin (Nisshin EM) following the methods of Morita et al. (2002). Ultrathin sections were cut (70- to 90-nm thick), stained with uranyl acetate and lead nitrate, and examined with a transmission electron microscope (JEM 2000FXII; JEOL).

Confocal Microscopy

Inflorescence stems segments were excised from 5-week-old plants and sectioned longitudinally and manually. The sections were observed using a confocal laser scanning microscope (FV1000; Olympus). Then, GFP fluorescence and chlorophyll autofluorescence were detected with 500- to 510-nm and 640- to 700-nm spectral settings, respectively, following a 488-nm excitation.

Molecular Cloning and Plant Transformation

For the complementation analysis, a 7.2-kb genomic DNA fragment of *ZIP3/VPS35A* including the 1.4-kb putative promoter region and the 0.3-kb 3' downstream region was amplified by PCR (primer set: gZIP3-F/gZIP3-R) using a BAC DNA T17A5 as a template and then cloned into the binary vector pBIN19 (GenBank accession number U09365). Total RNA was isolated from inflorescence stems with the RNeasy plant mini kit (Qiagen). cDNAs were synthesized using SuperScript II reverse transcriptase (Invitrogen). cDNA of *ZIP3/VPS35A* (primer set: cZIP3-F/cZIP3-R), *VPS35B* (primer set: cVPS35B-F/cVPS35B-R), and *VPS35C* (primer set: cVPS35C-F/cVPS35C-R) were amplified by PCR using synthesized cDNAs as templates and then cloned into pCR-Blunt II-TOPO vector (ZERO Blunt TOPO PCR cloning kit; Invitrogen). The resulting cDNA was inserted into the region between the *SCR* promoter and NOS terminator in pBIN19. The DNA sequence of each construct was confirmed by sequencing. The resulting constructs were transformed into *Agrobacterium tumefaciens* strain GV3101 (pMP90) and then introduced into *zip3-1 zig-1*

plants by the floral dip method (Clough and Bent, 1998). T1 plants were selected for resistance against kanamycin (30 $\mu\text{g}/\text{mL}$). Expression of transgenes (*SCRpro::ZIP3/VPS35A*, *VPS35B*, or *VPS35C*) was confirmed by RT-PCR analysis using primer sets that are able to specifically detect transcripts derived from the transgenes [primer sets: pSCR(-30)D/cZIP3-R2, pSCR(-30)D/cVPS35BR1, and pSCR(-30)D/cVPS35CR1]. The sequences of primers used are indicated in Supplemental Table 3 online.

Protein Extraction and Immunoprecipitation

Immunoprecipitation of detergent extracts from the shoots was performed as described previously (Yano et al., 2003), with minor modifications. Shoots (0.5 g) from 6-week-old plants without fruits were homogenized on ice in 10 mL of extraction buffer (50 mM HEPES-KOH, pH 6.5, 10 mM KOAc, 100 mM NaCl, 5 mM EDTA, and 0.4 M sucrose) with a protease inhibitor cocktail (Sigma-Aldrich). The homogenate was passed through Miracloth (Calbiochem) to remove debris. This extract was centrifuged at 15,000g for 30 min at 4°C. The pellet was resuspended in 1 mL of extraction buffer containing 1% (v/v) Triton X-100, protease inhibitor cocktail, and PreserveX-QML Polymeric Micelles (QBI Life Sciences) and then incubated at 4°C for 3 h with rotation. Insoluble material was removed by centrifugation at 10,000g for 10 min at 4°C. Protein concentration was determined with the BCA kit (Pierce) to use samples of equal protein amount for protein gel blot analysis or immunoprecipitation.

μ -MACS ProteinA MicroBeads (Miltenyi Biotec) were preincubated with anti-SYP22 antibody for at least 1 h at 4°C on the rotator. The beads were then added to the extract and incubated for at least 4 h at 4°C with rotation. The samples were applied to μ -Columns (Miltenyi Biotec) attached to the magnetic field of the μ -MACS separator (Miltenyi Biotec) and the flow-through was collected. Then, the column was washed five times with extraction buffer containing 1% (v/v) Triton X-100 and two times with PBS (130 mM NaCl, 7 mM Na_2HPO_4 , and 3 mM NaH_2PO_4 , pH 7.4). Protein (immunoprecipitate) was then eluted from the beads with 100 mL of SDS sample buffer. Equal volumes of total protein extract, flow-through, or immunoprecipitate were separated by SDS-PAGE followed by immunoblotting using anti-VTI12 antibody.

Accession Numbers

Sequence data from this article can be found in the GenBank/EMBL data libraries under the following accession numbers: *ZIG/VTI11*, At5g39510; *ZIP3/VPS35A*, At2g17790; *VPS35B*, At1g75850; *VPS35C*, At3g51310; *VPS26A*, At5g53530; *VPS26B*, At4g27690; and *MAIGO1/VPS29*, At3g47810. Accession numbers for T-DNA insertion lines are as follows: *zip3-3*, SALK_039689; *zip3-4*, SALK_125271, *vps35b*, SALK_014345; *vps35c*, SALK_099735; *vps26a*, GABI_053c12; and *vps26b*, SALK_142592.

Supplemental Data

The following materials are available in the online version of this article.

Supplemental Figure 1. Morphological Phenotype of *zip3-1 zig-1*.

Supplemental Figure 2. Phenotypes of Alleles of *zip3 zig-1* Double Mutants.

Supplemental Figure 3. Immunoblot Analysis of ZIP3/VPS35A Protein.

Supplemental Figure 4. Phenotypes of Alleles of *zip3* Single Mutants.

Supplemental Figure 5. Morphological Phenotypes of *mag1-1* and *mag1-1 zig-1* Mutants.

Supplemental Figure 6. Phenotypes of *vps26* Single Mutants.

Supplemental Figure 7. Phenotypes of *vps35b* and *vps35c* Single Mutants.

Supplemental Figure 5. Localization of GFP-VTI12 and ARA6-mRFP in Endodermal Cells.

Supplemental Table 1. Localization of Amyloplasts in the Endodermal Cell.

Supplemental Table 2. Quantitative Analysis of the Cytological Phenotype of Living Endodermal Cells Based on the Observation as Shown in Figures 3H to 3K.

Supplemental Table 3. Primer Sets for Cloning and RT-PCR

ACKNOWLEDGMENTS

We thank Natasha V. Raikhel for providing the anti-VTI12 antibody, Ikuko Hara-Nishimura for the anti-VPS35A antibody, Takashi Ueda and Tomohiro Uemura for valuable discussions, and Nauko Inui and Kaori Kaminoyama for technical assistance. We also thank the SALK Institute and the Max Planck Institute for Plant Breeding Research for providing T-DNA insertion mutant lines. The financial support of a Grant-in-Aid for Scientific Research from the Ministry of Education, Science, Sports, and Culture of Japan (16085205) and a grant from the Bioarchitect Project of RIKEN (to M.T.M.) is gratefully acknowledged.

Received June 11, 2009; revised November 6, 2009; accepted December 14, 2009; published January 19, 2010.

REFERENCES

- Bassham, D.C., Sanderfoot, A.A., Kovaleva, V., Zheng, H., and Raikhel, N.V. (2000). AtVPS45 complex formation at the trans-Golgi network. *Mol. Biol. Cell* **11**: 2251–2265.
- Bonifacino, J.S., and Hurley, J.H. (2008). Retromer. *Curr. Opin. Cell Biol.* **20**: 427–436.
- Bonifacino, J.S., and Rojas, R. (2006). Retrograde transport from endosomes to the trans-Golgi network. *Nat. Rev. Mol. Cell Biol.* **7**: 568–579.
- Cai, H., Reinisch, K., and Ferro-Novick, S. (2007). Coats, tethers, Rabs, and SNAREs work together to mediate the intracellular destination of a transport vesicle. *Dev. Cell* **12**: 671–682.
- Canuel, M., Lefrancois, S., Zeng, J., and Morales, C.R. (2008). AP-1 and retromer play opposite roles in the trafficking of sortilin between the Golgi apparatus and the lysosomes. *Biochem. Biophys. Res. Commun.* **366**: 724–730.
- Clough, S.J., and Bent, A.F. (1998). Floral dip: a simplified method for Agrobacterium-mediated transformation of *Arabidopsis thaliana*. *Plant J.* **16**: 735–743.
- Collins, B.M. (2008). The structure and function of the retromer protein complex. *Traffic* **9**: 1811–1822.
- Collins, B.M., Norwood, S.J., Kerr, M.C., Mahony, D., Seaman, M.N., Teasdale, R.D., and Owen, D.J. (2008). Structure of Vps26B and mapping of its interaction with the retromer protein complex. *Traffic* **9**: 366–379.
- Dacks, J.B., and Field, M.C. (2007). Evolution of the eukaryotic membrane-trafficking system: Origin, tempo and mode. *J. Cell Sci.* **120**: 2977–2985.
- Dacks, J.B., Poon, P.P., and Field, M.C. (2008). Phylogeny of endocytic

- components yields insight into the process of nonendosymbiotic organelle evolution. *Proc. Natl. Acad. Sci. USA* **105**: 588–593.
- Ebine, K., Okatani, Y., Uemura, T., Goh, T., Shoda, K., Niihama, M., Morita, M.T., Spitzer, C., Otegui, M.S., Nakano, A., and Ueda, T.** (2008). A SNARE complex unique to seed plants is required for protein storage vacuole biogenesis and seed development of *Arabidopsis thaliana*. *Plant Cell* **20**: 3006–3021.
- Fasshauer, D., Sutton, R.B., Brunger, A.T., and Jahn, R.** (1998). Conserved structural features of the synaptic fusion complex: SNARE proteins reclassified as Q- and R-SNAREs. *Proc. Natl. Acad. Sci. USA* **95**: 15781–15786.
- Fukaki, H., Fujisawa, H., and Tasaka, M.** (1996). SGR1, SGR2, SGR3: Novel genetic loci involved in shoot gravitropism in *Arabidopsis thaliana*. *Plant Physiol.* **110**: 945–955.
- Fukaki, H., Wysocka-Diller, J., Kato, T., Fujisawa, H., Benfey, P.N., and Tasaka, M.** (1998). Genetic evidence that the endodermis is essential for shoot gravitropism in *Arabidopsis thaliana*. *Plant J.* **14**: 425–430.
- Haft, C.R., Sierra, M.L., Bafford, R., Lesniak, M.A., Barr, V.A., and Taylor, S.I.** (2000). Human orthologs of yeast vacuolar protein sorting proteins Vps26, Vps29, and Vps35: Assembly into multimeric complexes. *Mol. Biol. Cell* **11**: 4105–4116.
- Hierro, A., Rojas, A.L., Rojas, R., Murthy, N., Effantin, G., Kajava, A. V., Steven, A.C., Bonifacino, J.S., and Hurley, J.H.** (2007). Functional architecture of the retromer cargo-recognition complex. *Nature* **449**: 1063–1067.
- Horazdovsky, B.F., Davies, B.A., Seaman, M.N., McLaughlin, S.A., Yoon, S., and Emr, S.D.** (1997). A sorting nexin-1 homologue, Vps5p, forms a complex with Vps17p and is required for recycling the vacuolar protein-sorting receptor. *Mol. Biol. Cell* **8**: 1529–1541.
- Jaillais, Y., Fobis-Loisy, I., Miège, C., Rollin, C., and Gaude, T.** (2006). AtSNX1 defines an endosome for auxin-carrier trafficking in *Arabidopsis*. *Nature* **443**: 106–109.
- Jaillais, Y., Santambrogio, M., Rozier, F., Fobis-Loisy, I., Miège, C., and Gaude, T.** (2007). The retromer protein VPS29 links cell polarity and organ initiation in plants. *Cell* **130**: 1057–1070.
- Kanamori, T., Inoue, T., Sakamoto, T., Gengyo-Ando, K., Tsujimoto, M., Mitani, S., Sawa, H., Aoki, J., and Arai, H.** (2008). Beta-catenin asymmetry is regulated by PLA1 and retrograde traffic in *C. elegans* stem cell divisions. *EMBO J.* **27**: 1647–1657.
- Kato, T., Morita, M.T., Fukaki, H., Yamauchi, Y., Uehara, M., Niihama, M., and Tasaka, M.** (2002). SGR2, a phospholipase-like protein, and ZIG/SGR4, a SNARE, are involved in the shoot gravitropism of *Arabidopsis*. *Plant Cell* **14**: 33–46.
- Kurten, R.C., Cadena, D.L., and Gill, G.N.** (1996). Enhanced degradation of EGF receptors by a sorting nexin, SNX1. *Science* **272**: 1008–1010.
- Morita, M.T., Kato, T., Nagafusa, K., Saito, C., Ueda, T., Nakano, A., and Tasaka, M.** (2002). Involvement of the vacuoles of the endodermis in the early process of shoot gravitropism in *Arabidopsis*. *Plant Cell* **14**: 47–56.
- Morita, M.T., and Tasaka, M.** (2004). Gravity sensing and signaling. *Curr. Opin. Plant Biol.* **7**: 712–718.
- Niihama, M., Uemura, T., Saito, C., Nakano, A., Sato, M.H., Tasaka, M., and Morita, M.T.** (2005). Convergence of functional specificity in Qb-SNARE VTI1 homologues of *Arabidopsis*. *Curr. Biol.* **15**: 555–560.
- Nothwehr, S.F., Bruinsma, P., and Strawn, L.A.** (1999). Distinct domains within Vps35p mediate the retrieval of two different cargo proteins from the yeast prevacuolar/endosomal compartment. *Mol. Biol. Cell* **10**: 875–890.
- Nothwehr, S.F., Ha, S.A., and Bruinsma, P.** (2000). Sorting of yeast membrane proteins into an endosome-to-Golgi pathway involves direct interaction of their cytosolic domains with Vps35p. *J. Cell Biol.* **151**: 297–310.
- Nothwehr, S.F., and Hines, A.E.** (1997). The yeast VPS5/GRD2 gene encodes a sorting nexin-1-like protein required for localizing membrane proteins to the late Golgi. *J. Cell Sci.* **110**: 1063–1072.
- Oliviusson, P., Heinzerling, O., Hillmer, S., Hinz, G., Tse, Y.C., Jiang, L., and Robinson, D.G.** (2006). Plant retromer, localized to the prevacuolar compartment and microvesicles in *Arabidopsis*, may interact with vacuolar sorting receptors. *Plant Cell* **18**: 1239–1252.
- Reddy, J.V., and Seaman, M.N.** (2001). Vps26p, a component of retromer, directs the interactions of Vps35p in endosome-to-Golgi retrieval. *Mol. Biol. Cell* **12**: 3242–3256.
- Rojas, R., Kametaka, S., Haft, C.R., and Bonifacino, J.S.** (2007). Interchangeable but essential functions of SNX1 and SNX2 in the association of retromer with endosomes and the trafficking of mannose 6-phosphate receptors. *Mol. Cell. Biol.* **27**: 1112–1124.
- Rojas, R., van Vlijmen, T., Mardones, G.A., Prabhu, Y., Rojas, A.L., Mohammed, S., Heck, A.J., Raposo, G., van der Sluijs, P., and Bonifacino, J.S.** (2008). Regulation of retromer recruitment to endosomes by sequential action of Rab5 and Rab7. *J. Cell Biol.* **183**: 513–526.
- Rojo, E., and Denecke, J.** (2008). What is moving in the secretory pathway of plants? *Plant Physiol.* **147**: 1493–1503.
- Rutherford, S., and Moore, I.** (2002). The *Arabidopsis* Rab GTPase family: Another enigma variation. *Curr. Opin. Plant Biol.* **5**: 518–528.
- Sack, F.D.** (1991). Plant gravity sensing. *Int. Rev. Cytol.* **127**: 193–252.
- Saito, C., Morita, M.T., Kato, T., and Tasaka, M.** (2005). Amyloplasts and vacuolar membrane dynamics in the living graviperceptive cell of the *Arabidopsis* inflorescence stem. *Plant Cell* **17**: 548–558.
- Sanderfoot, A.** (2007). Increases in the number of SNARE genes parallels the rise of multicellularity among the green plants. *Plant Physiol.* **144**: 6–17.
- Sanderfoot, A.A., Kovaleva, V., Bassham, D.C., and Raikhel, N.V.** (2001). Interactions between syntaxins identify at least five SNARE complexes within the Golgi/prevacuolar system of the *Arabidopsis* cell. *Mol. Biol. Cell* **12**: 3733–3743.
- Sanderfoot, A.A., Kovaleva, V., Zheng, H., and Raikhel, N.V.** (1999). The t-SNARE AtVAM3p resides on the prevacuolar compartment in *Arabidopsis* root cells. *Plant Physiol.* **121**: 929–938.
- Sato, M.H., Nakamura, N., Ohsumi, Y., Kouchi, H., Kondo, M., Hara-Nishimura, I., Nishimura, M., and Wada, Y.** (1997). The AtVAM3 encodes a syntaxin-related molecule implicated in the vacuolar assembly in *Arabidopsis thaliana*. *J. Biol. Chem.* **272**: 24530–24535.
- Schmid, M., Davison, T.S., Henz, S.R., Pape, U.J., Demar, M., Vingron, M., Schölkopf, B., Weigel, D., and Lohmann, J.U.** (2005). A gene expression map of *Arabidopsis thaliana* development. *Nat. Genet.* **37**: 501–506.
- Seaman, M.N.** (2005). Recycle your receptors with retromer. *Trends Cell Biol.* **15**: 68–75.
- Seaman, M.N.** (2007). Identification of a novel conserved sorting motif required for retromer-mediated endosome-to-TGN retrieval. *J. Cell Sci.* **120**: 2378–2389.
- Seaman, M.N., Marcusson, E.G., Cereghino, J.L., and Emr, S.D.** (1997). Endosome to Golgi retrieval of the vacuolar protein sorting receptor, Vps10p, requires the function of the VPS29, VPS30, and VPS35 gene products. *J. Cell Biol.* **137**: 79–92.
- Seaman, M.N., McCaffery, J.M., and Emr, S.D.** (1998). A membrane coat complex essential for endosome-to-Golgi retrograde transport in yeast. *J. Cell Biol.* **142**: 665–681.
- Shimada, T., Koumoto, Y., Li, L., Yamazaki, M., Kondo, M., Nishimura, M., and Hara-Nishimura, I.** (2006). AtVPS29, a putative component of a retromer complex, is required for the efficient sorting of seed storage proteins. *Plant Cell Physiol.* **47**: 1187–1194.
- Shimoi, W., Ezawa, I., Nakamoto, K., Uesaki, S., Gabreski, G., Aridor, M., Yamamoto, A., Nagahama, M., Tagaya, M., and Tani,**

- K. (2005). p125 is localized in endoplasmic reticulum exit sites and involved in their organization. *J. Biol. Chem.* **280**: 10141–10148.
- Silady, R.A., Ehrhardt, D.W., Jackson, K., Faulkner, C., Oparka, K., and Somerville, C.R.** (2008). The GRV2/RME-8 protein of *Arabidopsis* functions in the late endocytic pathway and is required for vacuolar membrane flow. *Plant J.* **53**: 29–41.
- Silady, R.A., Kato, T., Lukowitz, W., Sieber, P., Tasaka, M., and Somerville, C.R.** (2004). The gravitropism defective 2 mutants of *Arabidopsis* are deficient in a protein implicated in endocytosis in *Caenorhabditis elegans*. *Plant Physiol.* **136**: 3095–3103, discussion 3002.
- Surpin, M., Zheng, H., Morita, M.T., Saito, C., Avila, E., Blakeslee, J.J., Bandyopadhyay, A., Kovaleva, V., Carter, D., Murphy, A., Tasaka, M., and Raikhel, N.** (2003). The VTI family of SNARE proteins is necessary for plant viability and mediates different protein transport pathways. *Plant Cell* **15**: 2885–2899.
- Tamura, K., Takahashi, H., Kunieda, T., Fuji, K., Shimada, T., and Hara-Nishimura, I.** (2007). *Arabidopsis* KAM2/GRV2 is required for proper endosome formation and functions in vacuolar sorting and determination of the embryo growth axis. *Plant Cell* **19**: 320–332.
- Uemura, T., Ueda, T., Ohniwa, R.L., Nakano, A., Takeyasu, K., and Sato, M.H.** (2004). Systematic analysis of SNARE molecules in *Arabidopsis*: Dissection of the post-Golgi network in plant cells. *Cell Struct. Funct.* **29**: 49–65.
- Wysocka-Diller, J.W., Helariutta, Y., Fukaki, H., Malamy, J.E., and Benfey, P.N.** (2000). Molecular analysis of SCARECROW function reveals a radial patterning mechanism common to root and shoot. *Development* **127**: 595–603.
- Yamauchi, Y., Fukaki, H., Fujisawa, H., and Tasaka, M.** (1997). Mutations in the SGR4, SGR5 and SGR6 loci of *Arabidopsis thaliana* alter the shoot gravitropism. *Plant Cell Physiol.* **38**: 530–535.
- Yamazaki, M., Shimada, T., Takahashi, H., Tamura, K., Kondo, M., Nishimura, M., and Hara-Nishimura, I.** (2008). *Arabidopsis* VPS35, a retromer component, is required for vacuolar protein sorting and involved in plant growth and leaf senescence. *Plant Cell Physiol.* **49**: 142–156.
- Yano, D., Sato, M., Saito, C., Sato, M.H., Morita, M.T., and Tasaka, M.** (2003). A SNARE complex containing SGR3/AtVAM3 and ZIG/VTI11 in gravity-sensing cells is important for *Arabidopsis* shoot gravitropism. *Proc. Natl. Acad. Sci. USA* **100**: 8589–8594.
- Zheng, H., von Mollard, G.F., Kovaleva, V., Stevens, T.H., and Raikhel, N.V.** (1999). The plant vesicle-associated SNARE AtVTI1a likely mediates vesicle transport from the trans-Golgi network to the prevacuolar compartment. *Mol. Biol. Cell* **10**: 2251–2264.